

# Modelling creep of high strength concrete

D. Dias-da-Costa\* and E.N.B.S. Júlio

*ISISE, Department of Civil Engineering, University of Coimbra, Rua Luís Reis Santos,  
Universidade de Coimbra - Pólo II, 3030-290 Coimbra, Portugal*

*(Received April 28, 2009, Accepted August 21, 2010)*

**Abstract.** Recent developments in concrete mixing made possible the production of concretes with high compressive strength showing, simultaneously, high workability. These concretes also present high strengths at young ages, allowing the application of loads sooner. It is of fundamental importance to verify if creep models developed for current concrete still apply to these new concretes. First, a FEM-based software was adopted to test available creep models, most used for normal strength concrete, considering examples with known analytical results. Several limitations were registered, resulting in an incorrect simulation of three-dimensional creep. Afterwards, it was implemented a Kelvin-chain algorithm allowing the use of a chosen number of elements, which adequately simulated the adopted examples. From the comparison between numerical and experimental results, it was concluded that the adopted algorithm can be used to model creep of high strength concrete, if the material properties are previously experimentally assessed.

**Keywords:** high strength concrete; creep; numerical modeling; kelvin-chain.

---

## 1. Introduction

Subjected to permanent loading, concrete specimens exhibit an immediate (elastic) deformation, followed by a delayed deformation, due to creep and shrinkage of different types. When hygrometric equilibrium is attained before loading, by preventing any moisture loss to the environment, basic creep occurs. If drying is possible, additional drying creep takes place (Acker and Ulm 2001).

Once water is added to the remaining concrete constituents, the cement hydration leads to chemical shrinkage. Furthermore, cement hydration is a highly exothermic reaction leading to a contraction of the concrete mass when cooling takes place, thus causing thermal shrinkage. Before hardening, settlement of fresh concrete and water drying from the surface causes plastic shrinkage. After curing, if the surfaces are not isolated from the environment, shrinkage by carbonation of the superficial hydrated cement paste occurs. Finally, autogeneous shrinkage is justified by a gradual conversion of free water into combined, adsorbed or interlayer water.

With recent progress in concrete mixing, implying the use of pozzolanic additions, higher quality cements and third generation superplastifiers, it became possible to produce high workability high strength concrete (HSC). Since high compressive strengths are observed at young ages, loads can be applied earlier. Being HSC significantly different from current concrete and since very distinct loading conditions can be observed, it is relevant to experimentally characterize the time-dependent behaviour of these new concretes and to verify if existing creep models, validated for current concrete, can still be used to simulate their behaviour. Although recently advanced creep models for

---

\* Corresponding author, Assistant Professor, E-mail: [dcosta@dec.uc.pt](mailto:dcosta@dec.uc.pt)

the simulation of early-age concrete behaviour (Pichler 2008) and nonlinear basic creep (Bockhold 2007) have been proposed, the study herein described only considers a simplified approach. Moreover, shrinkage is not considered in the study herein described since in high strength concrete, due to a low water-binding ratio, this is not significant.

In this paper, Cast3m, a Finite Element Method (FEM) based code developed by Centre for Atomic Energy, in France, was adopted to test creep models, considering simple examples with known solutions. A linear viscoelastic (LVE) algorithm, originally developed by Bazant (Bazant and Wittmann 1982) for current concrete creep analysis, was implemented in Cast3m and applied to simulating creep in both current concrete and HSC. Results and major conclusions drawn from the study are presented.

## 2. Numerical modelling of concrete creep

The potentialities and limitations of creep models for current concrete were assessed considering simple examples with permanent and variable loading; isotropic loading; and material ageing, for which a linear viscoelastic algorithm (LVE) was implemented (Bazant and Wittmann 1982).

### 2.1 Strain hardening algorithm

Strain hardening (SH) relates the creep rate at a time  $t$  with the total creep since the start of loading, given by the following equation and represented in Fig. 1

$$\frac{d\varepsilon}{dt} = f(\sigma, \varepsilon_c) \quad (1)$$

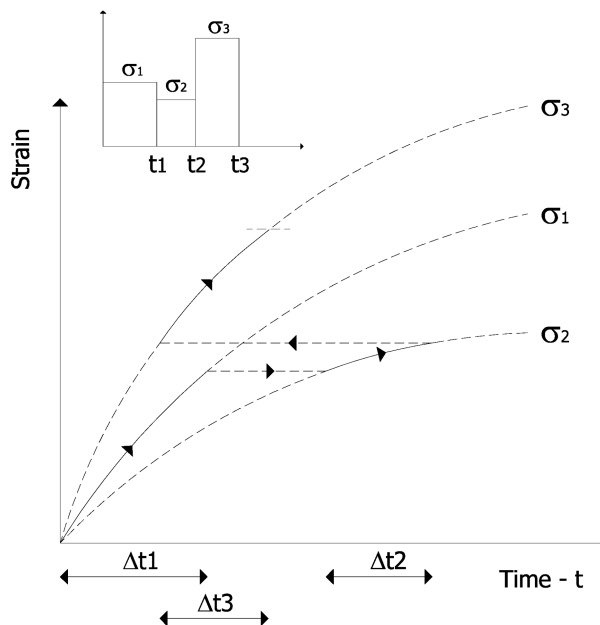


Fig. 1 Strain hardening procedure for variable stress

where  $\mathbf{f}$  is a function defining the rate of the creep.

SH can be used for increasing stresses but, for the inverse situation, it is not possible to determine a time  $t$ , with the applied stress, that would lead to the total observed creep strain (England 1967). Furthermore, Bazant (1987) proved that the equivalent time procedure is identical to the SH having similar advantages and problems.

This method can not simulate recovery situations and the obtained creep strains are larger than those calculated by a rate of creep method (England 1967, Bazant 1987). Another flaw of this method is that different stress histories, leading to the same stress and creep strain at a time  $t$ , would have, subsequently, the same creep evolution (Bazant 1987).

## 2.2 Viscoelastic algorithm with ageing

### 2.2.1 Equilibrium

Equilibrium between internal and external stresses must be guaranteed at all time instants. Having the state of equilibrium perfectly defined for the previous instant,  $t_b$ , it is intended to evaluate the equilibrium for the instant  $t_{t+\Delta t}$ . The vector of the unknown stresses for time  $t_{t+\Delta t}$ , represented by  ${}^{t+\Delta t}\boldsymbol{\sigma}$  in Eq. (2), is decomposed in a sum of a known stress vector,  ${}^t\boldsymbol{\sigma}$ , at time  $t_b$ , with  ${}^{\Delta t}\Delta\boldsymbol{\sigma}$  containing all unknown components of the stress increment (Borst and Sluys 1999)

$${}^{t+\Delta t}\boldsymbol{\sigma} = {}^t\boldsymbol{\sigma} + {}^{\Delta t}\Delta\boldsymbol{\sigma} . \quad (2)$$

Considering the equilibrium Eq. (3)

$$\int_V ({}^{t+\Delta t}\mathbf{B})^T {}^{t+\Delta t}\boldsymbol{\sigma} dv = {}^{t+\Delta t}\mathbf{f}_e \quad (3)$$

and replacing Eq. (3) at time  $t_{t+\Delta t}$  in Eq. (2), with the assumption that total strain increment,  ${}^{\Delta t}\Delta\boldsymbol{\varepsilon}$ , is a direct sum of elastic strain,  ${}^{\Delta t}\Delta\boldsymbol{\varepsilon}_e$ ; creep strain increment,  ${}^{\Delta t}\Delta\boldsymbol{\varepsilon}_v$ ; temperature strain; drying shrinkage; and other imposed strains increments,  ${}^{\Delta t}\Delta\boldsymbol{\varepsilon}_T$ , the incremental Eq. (4) can be obtained

$$\int_V ({}^{t+\Delta t}\mathbf{B})^T {}^{\Delta t}\Delta\boldsymbol{\sigma} dv = {}^{\Delta t}\Delta\mathbf{f}_e + {}^{\Delta t}\Delta\mathbf{f}_v + {}^{\Delta t}\Delta\mathbf{f}_T \quad (4)$$

in which

$${}^{\Delta t}\Delta\mathbf{f}_e = \int_V ({}^{t+\Delta t}\mathbf{B})^T {}^{\Delta t}\Delta\boldsymbol{\sigma} dv; \quad {}^{\Delta t}\Delta\mathbf{f}_v = \int_V ({}^{t+\Delta t}\mathbf{B})^T \mathbf{D}^{\Delta t}\Delta\boldsymbol{\varepsilon}_v dv; \quad {}^{\Delta t}\Delta\mathbf{f}_T = \int_V ({}^{t+\Delta t}\mathbf{B})^T \mathbf{D}^{\Delta t}\Delta\boldsymbol{\varepsilon}_T dv$$

being,  ${}^{\Delta t}\Delta\mathbf{f}_e$ , the nodal force variation equivalent to the external applied stress;  ${}^{\Delta t}\Delta\mathbf{f}_v$ , the nodal force variation equivalent to creep deformation;  ${}^{\Delta t}\Delta\mathbf{f}_T$ , the nodal force variation equivalent to temperature variation, drying shrinkage and other imposed strains; and  $\mathbf{B}$ , the matrix of deformations (Zienkiewicz and Taylor 1989).

To solve the system of nonlinear Eq (4), the Newton-Raphson method was adopted, implying a linearization of the equations. By linearizing the relation between the stress  ${}^{\Delta t}\Delta\boldsymbol{\sigma}$  and the nodal displacements increments  ${}^{\Delta t}\Delta\mathbf{d}$ , using the elasticity matrix  $\mathbf{D}$  and the matrix of deformations  $\mathbf{B}$ , Eq. (5) is obtained

$${}^{\Delta t}\Delta\boldsymbol{\sigma} = \mathbf{D} {}^{t+\Delta t}\mathbf{B} {}^{\Delta t}\Delta\mathbf{d} . \quad (5)$$

Combining Eqs. (4) and (5), Eq. (6) is established for the incremental displacements, being  ${}^{t+\Delta t}\mathbf{H}$

the stiffness matrix

$${}^{t+\Delta t}\mathbf{H}^{\Delta t}\Delta\mathbf{d} = \Delta t\Delta\mathbf{f}_e + \Delta t\Delta\mathbf{f}_v + \Delta t\Delta\mathbf{f}_T \quad (6)$$

with

$${}^{t+\Delta t}\mathbf{H} = \int_V ({}^{t+\Delta t}\mathbf{B})^T \mathbf{D} {}^{t+\Delta t}\mathbf{B} dv.$$

Material constitutive law is introduced by means of the elasticity matrix  $\mathbf{D}$  and creep strain increment  $\Delta t\Delta\boldsymbol{\varepsilon}_c$ , both present in Eq. (6) and determined in the following section.

### 2.2.2 Linear viscoelastic constitutive law with ageing and step-by-step integration

It is assumed that, for service conditions, concrete can be considered a linear viscoelastic ageing material (Bazant and Wittmann 1982). McHenry superposition principle (Neville 1959, Yue and Taerwe 1992, Gardner and Tsuruta 2004) is applied, considering the independency of creep strains produced by a unit stress applied at different ages (Gardner and Tsuruta 2004). Implicitly, it is assumed that tensile and compressive creep behave identically (Ross 1958), for the same stress normalized value. However, there is the possibility of using creep functions specifically developed for creep recovery (Yue 1992).

Eq. (7) can be written for the total strain at time  $t$

$$\boldsymbol{\varepsilon}(t) = \int_0^t \mathbf{J}(t, t') d\boldsymbol{\sigma}(t') + \boldsymbol{\varepsilon}_T(t) \quad (7)$$

where:  $\mathbf{J}(t, t')$  is the three-dimensional creep function, giving the strain at time  $t$  caused by a unit constant stress applied at time  $t'$ ;  $\boldsymbol{\sigma}(t')$  is the stress applied at instant  $t'$ ; and  $\boldsymbol{\varepsilon}_T(t)$  is a stress-independent inelastic strain originated by temperature variation, drying shrinkage and other imposed strains.

The three-dimensional creep function is related to the scalar creep function  $J(t, t')$  by Eq. (8), assuming isotropic material behaviour and assuming that the elastic Poisson ratio  $\mu$  does not vary with time, which is not absolutely accurate (Gopalakrishnan *et al.* 1969, Coutinho and Gonçalves 1988).

$$\mathbf{J}(t, t') = J(t, t')\bar{\mathbf{D}} = J(t, t') \begin{bmatrix} 1 & -\mu & -\mu & 0 & 0 & 0 \\ -\mu & 1 & -\mu & 0 & 0 & 0 \\ -\mu & -\mu & 1 & 0 & 0 & 0 \\ 0 & 0 & 0 & (1+\mu) & 0 & 0 \\ 0 & 0 & 0 & 0 & (1+\mu) & 0 \\ 0 & 0 & 0 & 0 & 0 & (1+\mu) \end{bmatrix}. \quad (8)$$

A scalar creep function can be approximated by a Dirichlet series, Eq. (9), which can be shown to be equivalent to a physical Kelvin-chain model (Bazant and Wittmann 1982)

$$J(t, t') = \frac{1}{E(t')} + \sum_{i=1}^n \frac{1}{\hat{E}_i(t')} \left( 1 - e^{-\frac{t-t'}{\tau_i}} \right) \quad (9)$$

where:  $E(t')$  is the Young modulus of concrete at age  $t'$ ;  $\hat{E}_i(t')$  and  $\tau_i$  are, respectively, the ageing coefficient and the retardation time for the Kelvin element.

Eq. (10) is deduced by inserting Eqs. (8) and (9) into Eq. (7)

$$\boldsymbol{\varepsilon}(t) - \boldsymbol{\varepsilon}_T(t) = \int_0^t \frac{1}{E(t')} \bar{\mathbf{D}} d\boldsymbol{\sigma}(t') + \sum_{i=1}^n \int_0^t \frac{1}{\hat{E}_i(t')} \left( 1 - e^{-\frac{t-t'}{\tau_i}} \right) \bar{\mathbf{D}} d\boldsymbol{\sigma}(t'). \quad (10)$$

This equation, or Eq. (7), can be solved by replacing the integrals by a discrete sum. However, there is a major computational cost for this procedure, since it becomes necessary to keep all stress history increments in each Gauss point. To overcome this limitation, it was adopted the following algorithm, LVE, originally developed by Bazant (Bazant and Wittmann 1982, Dias da Costa 2006).

According to this procedure, Eq. (10) is used in two successive instants,  $t_t$  and  $t_{t+\Delta t}$ , to obtain Eq. (11) for the strain variation  ${}^{\Delta t}\Delta\boldsymbol{\varepsilon} - {}^{\Delta t}\boldsymbol{\varepsilon}_T$

$$\begin{aligned} {}^{\Delta t}\Delta\boldsymbol{\varepsilon} - {}^{\Delta t}\boldsymbol{\varepsilon}_T &= \int_{t_t}^{t_{t+\Delta t}} \frac{1}{E(t')} \bar{\mathbf{D}} d\boldsymbol{\sigma}(t') + \sum_{i=1}^n \int_{t_t}^{t_{t+\Delta t}} \frac{1}{\hat{E}_i(t')} \bar{\mathbf{D}} d\boldsymbol{\sigma}(t') + \\ &+ \sum_{i=1}^n \int_0^{t_t} \frac{e^{-\frac{t_t-t'}{\tau_i}}}{\hat{E}_i(t')} \left( 1 - e^{-\frac{\Delta t}{\tau_i}} \right) \bar{\mathbf{D}} d\boldsymbol{\sigma}(t') - \sum_{i=1}^n \int_{t_t}^{t_{t+\Delta t}} \frac{e^{-\frac{t_{t+\Delta t}-t'}{\tau_i}}}{\hat{E}_i(t')} \bar{\mathbf{D}} d\boldsymbol{\sigma}(t'). \end{aligned} \quad (11)$$

Finally, using an arithmetic average between the initial and the final values in each time span,  $E(t')$  and  $\hat{E}_i(t')$  are now denoted by, respectively,  $E_{t+\frac{\Delta t}{2}}$  and  $(\hat{E}_i)_{t+\frac{\Delta t}{2}}$ . Also, with the assumption of linear stress variation in each time increment, Eq. (12) is developed for stress-strain law

$${}^{\Delta t}\Delta\boldsymbol{\sigma} = {}^{t+\Delta t}\overline{\mathbf{E}\mathbf{D}}^{-1} ({}^{\Delta t}\Delta\boldsymbol{\varepsilon} - {}^{\Delta t}\Delta\boldsymbol{\varepsilon}_v - {}^{\Delta t}\Delta\boldsymbol{\varepsilon}_T) \quad (12)$$

where

$${}^{\Delta t}\Delta\boldsymbol{\varepsilon}_v = \sum_{i=1}^n \left( 1 - e^{-\frac{\Delta t}{\tau_i}} \right) (\boldsymbol{\varepsilon}_i^*)_t \quad \text{and} \quad \frac{1}{{}^{t+\Delta t}\overline{E}} = \frac{1}{E_{t+\frac{\Delta t}{2}}} + \sum_{i=1}^n \frac{1 - \left( 1 - e^{-\frac{\Delta t}{\tau_i}} \right) \frac{\tau_i}{\Delta t}}{(\hat{E}_i)_{t+\frac{\Delta t}{2}}} \quad (13)$$

$$(\boldsymbol{\varepsilon}_i^*)_{t+\Delta t} = \frac{\bar{\mathbf{D}}^{\Delta t} \Delta\boldsymbol{\sigma} \left( 1 - e^{-\frac{\Delta t}{\tau_i}} \right) \frac{\tau_i}{\Delta t}}{(\hat{E}_i)_{t+\frac{\Delta t}{2}}} + (\boldsymbol{\varepsilon}_i^*)_t e^{-\frac{\Delta t}{\tau_i}}. \quad (14)$$

It should be noticed that only state parameters, defined in Eq. (14), need to be stored, one per Kelvin element and Gauss point, turning the computational procedure more efficient.

Finally the equilibrium Eq. (6) can be solved by replacing  ${}^{\Delta t}\Delta\boldsymbol{\varepsilon}_v$  and  $\mathbf{D}$  with  ${}^{\Delta t}\Delta\boldsymbol{\varepsilon}_v$  and  ${}^{t+\Delta t}\overline{\mathbf{E}\mathbf{D}}^{-1}$ , defined by Eq. (12) to Eq. (14), giving an unconditionally stable procedure (Bazant and Wittmann 1982).

### 2.2.3 Identification of the Dirichlet series coefficients

The coefficients of the Dirichlet series used for approximating creep function, Eq. (9), can be obtained by numerically adjusting experimental results available for high strength concrete. A

numerical procedure presented by Argyris *et al.* (Argyris and Silva 1992) was followed, using the least square method in minimizing the residual error of the approximation with iterative evaluation of the parameters with the Newton- Raphson method.

The measured specific creep strain (creep for a unit stress)  $\boldsymbol{\varepsilon}_v$  is a vector with  $m$  results. The Dirichlet series can be used to estimate the specific creep strains, represented in a vector  $\tilde{\boldsymbol{\varepsilon}}_v$ , which is a function  $\mathbf{f}(P_1, P_2, \dots, P_n)$  of the  $n$  Dirichlet viscoelastic parameters  $P_i$ . According to the previous considerations, the following expression can be used to evaluated the residual error vector  $\mathbf{e}$

$$\mathbf{e} = \boldsymbol{\varepsilon}_v - \tilde{\boldsymbol{\varepsilon}}_v. \quad (15)$$

By taking the Gaussian norm from Eq. (15), the error is minimized by solving Eq. (16) or the equivalent system of Eq. (17)

$$\frac{\partial \|\mathbf{e}\|}{\partial \mathbf{P}} = 2\mathbf{e}^T \frac{\partial \mathbf{e}}{\partial \mathbf{P}} = \mathbf{0}^T \quad (16)$$

$$\mathbf{G} = \left( \frac{\partial \tilde{\boldsymbol{\varepsilon}}_v}{\partial \mathbf{P}} \right)^T (\boldsymbol{\varepsilon}_v - \tilde{\boldsymbol{\varepsilon}}_v) = \mathbf{0} \quad (17)$$

where:  $\mathbf{P}$  is a vector of the coefficients; and  $\mathbf{0}$  is a  $n$ -dimensional zero vector (Argyris and Silva 1992).

If the delay time is also a parameter to be evaluated, the system of equations is nonlinear and can be solved using the Newton-Raphson method where, after some manipulation, the simple linear approximation, Eq. (18), emerges

$$\left( \frac{\partial \tilde{\boldsymbol{\varepsilon}}_v}{\partial \mathbf{P}} \right)^T \frac{\partial \tilde{\boldsymbol{\varepsilon}}_v}{\partial \mathbf{P}} \Delta \mathbf{P} = - \left( \frac{\partial \tilde{\boldsymbol{\varepsilon}}_v}{\partial \mathbf{P}} \right)^T (\boldsymbol{\varepsilon}_v - \tilde{\boldsymbol{\varepsilon}}_v). \quad (18)$$

Vector  $\mathbf{P}$  is successively approximated by evaluating  $\Delta \mathbf{P}$  from the system of Eq. (18), which is then replaced in Eq. (19)

$$\mathbf{P}_{i+1} = \mathbf{P}_i + \Delta \mathbf{P}. \quad (19)$$

### 2.3 Comparison of methods: testing examples

Virtually any structure, in its lifetime, experiences variable loading. However, experimental creep tests are usually performed on specimens subjected to constant stress and most numerical creep models were developed to simulate this situation. For this reason, a first example was considered using an eight node plane stress finite-element, subjected to constant and variable load situations, in order to analyse results for variable stress. Isotropic stress tensor is important to numerically model concrete creep (Coutinho and Gonçalves 1988). Therefore, a second example was considered using a twenty node hexahedron, subjected to an isotropic loading. Ageing is also an important factor mainly for HSC, since it is possible to apply loads sooner and since the rheological properties, by cement hydration, experience major changes in the first days of age. For that reason, a third example was considered consisting on a simplified ageing model using the same finite-element adopted on the previous example, subjected to a sudden change of the parameters of the Dirichlet series.

In order to compare both algorithms, a single Kelvin element was used (Dias-da-Costa 2006),

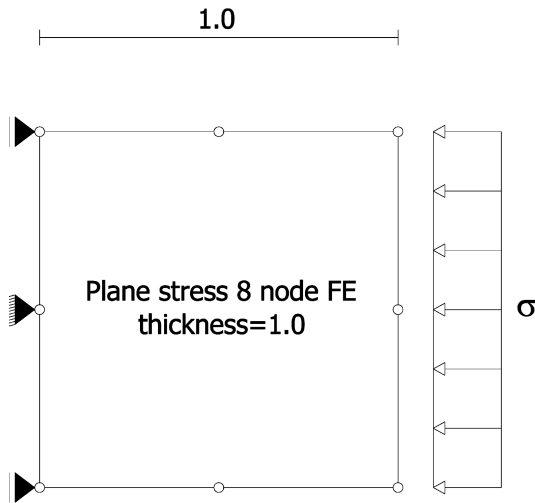


Fig. 2 Support and loading condition of the finite-element

although this is usually insufficient and more Kelvin-chain elements have to be used (Freudenthal and Roll 1958, Illston 1968, Bazant and Prasanna 1989).

### 2.3.1 First example – variable loading conditions

An eight node finite-element was analysed considering the support and loading conditions represented in Fig. 2. A Poisson ratio of 0.2, a Young modulus of 55.9 GPa and a scalar creep compliance determined according to Eq. (20) were considered. These values were obtained from the experimental study presented in Fernandes (2006) and Dias-da-Costa (2006)

$$\varepsilon_v = \frac{\sigma}{2.87406 \times 10^{10}} \left( 1 - e^{-\frac{t-t'}{3.92372}} \right) \quad (20)$$

being:  $\varepsilon_v$ , the scalar creep strain;  $\sigma$  [Pa], the stress applied at age  $t'$  [days], according to the time law represented in Fig. 3; and  $t$  [days], the instant of analysis.

A time period of 100 days was considered, being the load applied at the beginning. After 50 days, when creep deformation from the first stage is stabilized, changes are applied, according to Fig. 3, in constant stress, increasing stress, partial and complete unloading, and partial stress reversal.

The theoretical solution was obtained by applying the principle of superposition and Eq. (20). Small time steps were chosen when creep strain variation was most significant, being gradually increased after that. Similar approach has been adopted in the remaining test examples.

The results are represented in Fig. 3, being concluded that SH can be used for situations of constant or increasing stress. However, because creep strains are plastic and not recoverable, SH method is unable to predict any creep recovery. LVE algorithm is almost coincident with the theoretical solution for any stress history.

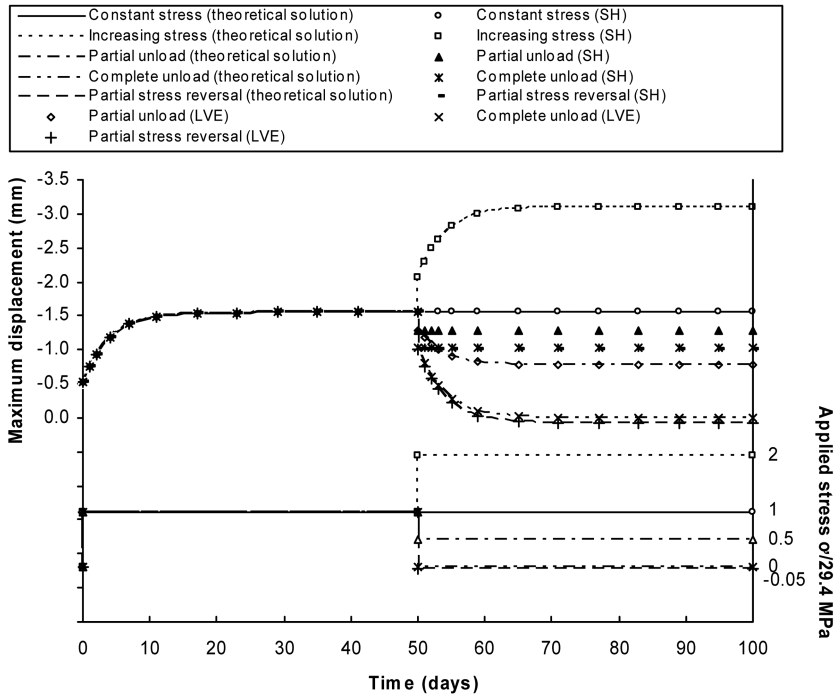


Fig. 3 Loading history of the finite-element and maximum axial displacement in the time domain

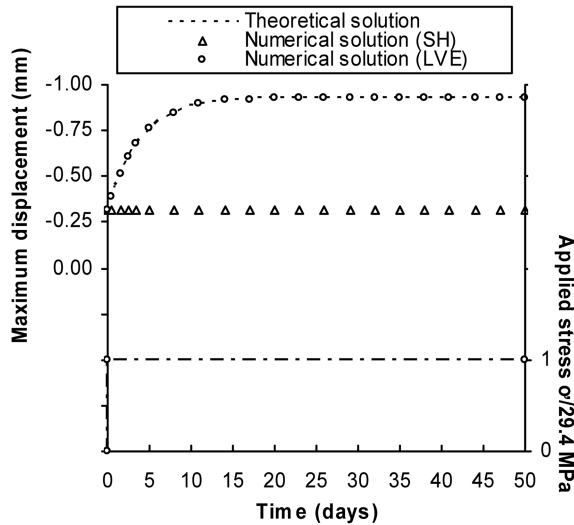


Fig. 4 Loading history of the finite-element and maximum axial displacement in the time domain

### 2.3.2 Second example – Isotropic loading

All material properties adopted in the first example were adopted, and an isotropic and uniform stress of 29.4 MPa was applied to a twenty node hexahedron, with unitary dimensions. A time interval of 50 days was considered with constant stress, as represented in Fig. 4.

The theoretical solution is given by Eq. (21), where  $\varepsilon$  is the scalar total strain,  $\sigma$  [Pa] is the applied stress, and  $t$  [days] is the instant of analysis.

$$t \geq 0: \varepsilon = (1 - 2 \times 0.2) \left[ \frac{\sigma}{55.885 \times 10^9} + \frac{\sigma}{2.87406 \times 10^{10}} \left( 1 - e^{-\frac{t}{3.92372}} \right) \right] \quad (21)$$

Fig. 4 represents the previous equation, with the numerical solution from SH and LVE algorithm. From result analysis it can be concluded that LVE algorithm (Bazant and Wittmann 1982) presents a numerical solution almost coincident with Eq. (21), while SH is unable to predict creep. This fact can be explained by the assumption of creep strain rate as exclusively proportional to the deviatoric stress tensor.

### 2.3.3 Third example – variable load and ageing

The same finite-element of the first example is considered, in the same conditions represented in Fig. 2. To simulate the gradual hydration of the anhydrous cement paste, inducing an ageing process and rheological evolution with time, it is assumed that all rheological changes are concentrated at the 10<sup>th</sup> day of the analysis. Until that age, the model has the same Young modulus and scalar creep function considered in the previous section. After the 10<sup>th</sup> day, the Young modulus is doubled and scalar creep is reduced to half.

The analysis is performed during 50 days being the stress applied at the first instant of the time interval. The stress is doubled according to the loading history represented in Fig. 5, while the rheological properties are changed according to the previous explanation.

The theoretical solution is determined by using the principle of superposition, leading to Eqs. (22) and (23)

$$0 \leq t \leq 10: \varepsilon = \frac{\sigma}{55.885 \times 10^9} + \frac{\sigma}{2.87406 \times 10^{10}} \left( 1 - e^{-\frac{t}{3.92372}} \right) \quad (22)$$

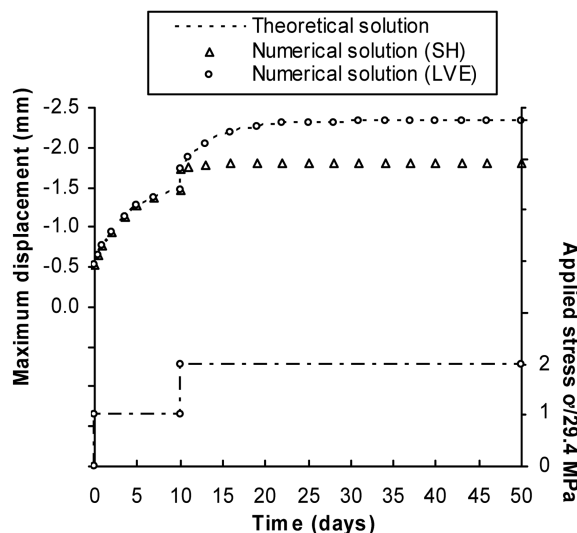


Fig. 5 Loading history of the finite-element and maximum axial displacement in the time domain

$$\begin{aligned}
 t > 10: \varepsilon = & \frac{\sigma}{55.885 \times 10^9} + \frac{\sigma}{2.87406 \times 10^{10}} \left( 1 - e^{-\frac{t}{3.92372}} \right) + \\
 & + \frac{\sigma}{111.770 \times 10^9} + \frac{\sigma}{5.74812 \times 10^{10}} \left( 1 - e^{-\frac{t-10}{3.92372}} \right)
 \end{aligned} \tag{23}$$

where:  $\varepsilon$  is the scalar total strain;  $\sigma$  [Pa] is the stress applied; and  $t$  [days] is the instant of analysis.

Theoretical results of Eqs. (22) and (23), as well as the numerical results obtained with SH and LVE algorithms, are represented in Fig. 5.

It was previously shown that SH procedure gives reliable results in increasing stress situations but, with ageing, the numerically computed strains are smaller than the expected values. After the 10<sup>th</sup> day of age there is a creep evolution similar to that shown in Fig. 3, for constant stress. SH revealed to be unable to consider the ageing process, which can be significant for young concrete loaded at early ages.

LVE algorithm results are almost identical to the theoretical values, showing that this algorithm can adequately consider the ageing process in this simplified situation (Bazant and Wittmann 1982).

#### 2.4 Definition of the proposed creep model

Several simple tests were proposed to compare SH and LVE algorithms. Concerning the loading condition, it was verified that SH can simulate creep only for constant or increasing stress situations, being unable to conveniently simulate creep recovery and stress inversion situations, where SH procedure implies that creep strain are plastic and not recoverable. Moreover, this algorithm assumes creep strain rate to be proportional to the deviatoric stress tensor and, therefore, is not suitable for concrete (Coutinho and Gonçalves 1988).

In relation to the rheological properties of concrete, mainly ageing, it was verified that this is not satisfactorily simulated by SH algorithm, which can be an important limitation for high strength concrete.

For all reasons previously referred to, SH does not accurately simulate creep for the majority of situations found in practice, either for current or high strength concrete. LVE algorithm, presented accurate results for all examples considered, concerning both loading and material properties changes, almost coincident with the theoretical solutions.

### 3. Simulation of HSC creep tests

Experimental tests were performed on prismatic specimens of high strength concrete to quantify the elastic deformation and the time-dependant deformation due to shrinkage and creep. The algorithms previously tested with simple examples are now used to numerically model these tests. First, LVE algorithm is used with only one Kelvin element. Then, more Kelvin-chain elements are introduced to increase the accuracy of the model. Finally, by comparing numerical and experimental results, the algorithm is validated for creep modelling of high strength concrete.

3.1 Material, methods and results

The following mix proportions per cubic meter of concrete were adopted (Fernandes 2006): 500 kg of type I:52.5 R Portland cement, 50 kg of silica fume, 1167 kg of washed siliceous sand with 4.24 fineness modulus, 532 kg of siliceous crushed aggregates with 6.47 fineness modulus, 144l of water, and 11.02 kg of a water reducing admixture.

Fig. 6 shows the equipment used in the experimental study to assess the material properties, according to Portuguese Standards (LNEC E 397 1993, LNEC E 398 1993, LNEC E 399 1993). The compressive strength was evaluated using standard cubic specimens with 150 mm and the Young modulus was measured using prismatic specimens with 150×150×600 mm<sup>3</sup>, Fig. 7. Shrinkage was measured in two prismatic specimens of 150×150×600 mm<sup>3</sup>, without external loading, while creep was assessed by computing the additional deformation in two identical specimens also subjected to a compressive stress of 29.4 MPa - Fig. 6 (Fernandes 2006). The results are represented in Fig. 8.

Creep tests were modelled using hexahedron finite-elements, with eight nodes, according to the mesh represented in Fig. 9, which was verified to be accurate (Dias-da-Costa 2006). The lower surface of the mesh is restrained from any displacement, while a constraint is applied to the upper surface in order to obtain equal vertical displacements.

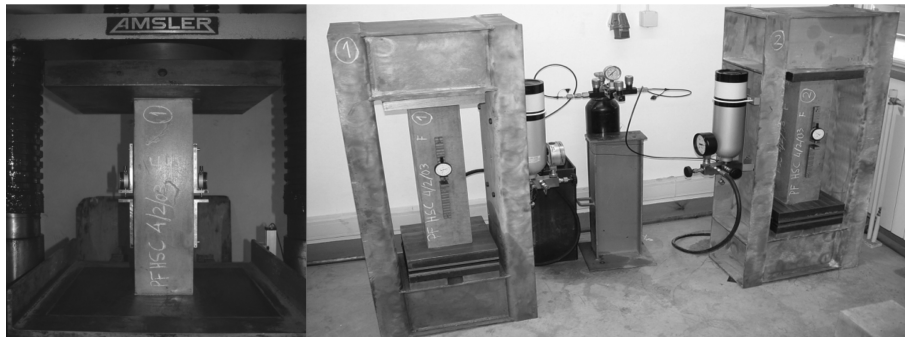


Fig. 6 (a) Equipment for evaluating compressive strength and Young modulus and (b) creep tests equipment

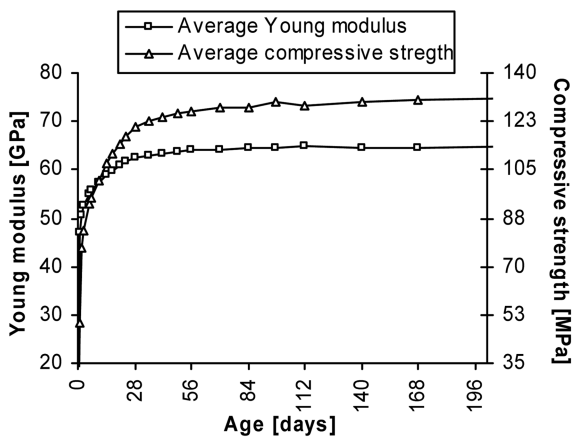


Fig. 7 Young modulus and compressive strength

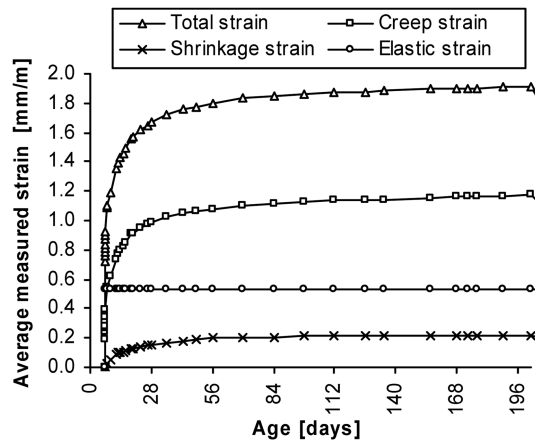


Fig. 8 Time-dependent behaviour for 29.4 MPa stress applied at 7 days of age

A constant compressive stress of 29.4 MPa was applied at 7 days of age according to Fig. 8. Due to limitations of the experimental set-up, ageing is not computed. As a direct consequence, in the numerical simulation, a constant Young modulus of 55.9 GPa was considered, obtained using the data represented in Fig. 7, with a Poisson ratio of 0.2.

### 3.2 Numerical results

#### 3.2.1 One Kelvin element

Argyris *et al.* (1992) algorithm presented in section §2.1.3 was used to numerically adjust creep results of Fig. 8, leading to Eq. (24). Only two complete periods of 28 days were considered because it

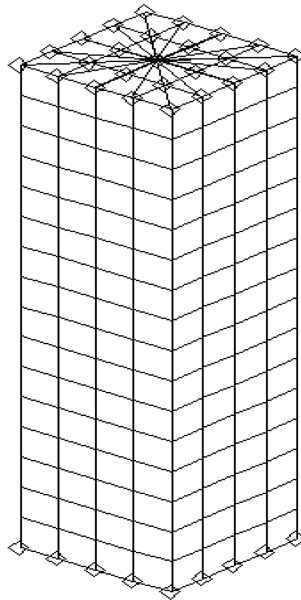


Fig. 9 Adopted mesh in all numerical simulations

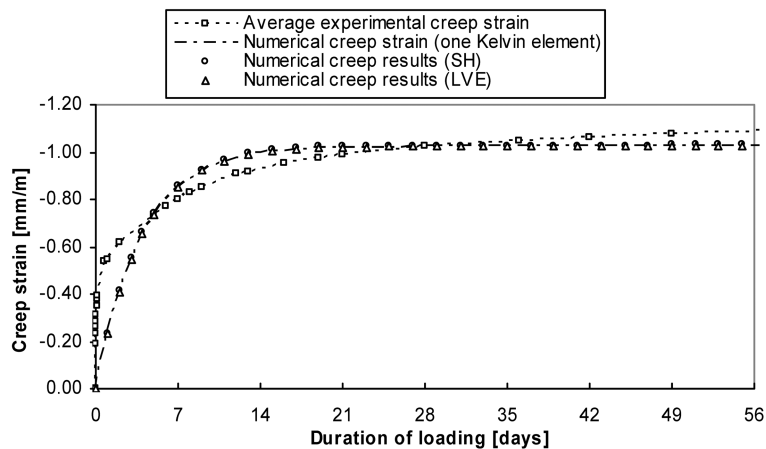


Fig. 10 Average experimental results and numerical results for creep strain for the first 56 days of loading

was not possible to satisfactorily adjust one Kelvin element to a larger time domain, Fig. 10.

$$C(t,t') = \frac{1}{2.87406 \times 10^{10}} \left( 1 - e^{-\frac{(t-t')}{3.92372}} \right) \quad (24)$$

where:  $C$  represents the scalar creep compliance at instant  $t$  [days] produced by a unitary stress (1 MPa) applied at instant  $t' = 7$  [days].

SH and LVE algorithms have similar numerical values (Fig. 10), because the stress is almost constant through the specimen. However, the approximation with one Kelvin element is limited and the numerical results can have significant differences from the observed values – Fig. 10.

### 3.2.2 Three Kelvin-chain elements

More Kelvin-chain elements were introduced to improve the accuracy of the numerical simulation. Argyris *et al.* (1992) algorithm was applied again, to obtain Eq. (25). The period of analysis was extended to cover all available data (196 days), being worth noting that if this period increases, more Kelvin-chain elements can be added to improve the results at later stages. However, for the available time domain, the number of used Kelvin-chain elements is sufficient to obtain good agreement with experimental creep strain Fig. 11.

$$C(t,t') = \frac{1}{9.43084219 \times 10^{10}} (1 - e^{-1197.417662(t-t')}) + \frac{1}{6.04722617 \times 10^{10}} (1 - e^{-0.4357843992(t-t')}) + \frac{1}{8.03848594 \times 10^{10}} (1 - e^{-0.03088288464(t-t')}) \quad (25)$$

where:  $C$  represents the scalar creep at instant  $t$  [days] produced by a unitary stress (1 MPa) applied at instant  $t' = 7$  [days].

Fig. 11 presents LVE results revealing good accuracy with the experimental average results in all time instants. That is justified by the fact that a sufficient number of Kelvin-chain elements have been used in the numerical approach, allowing to numerically reproduce the creep tests.

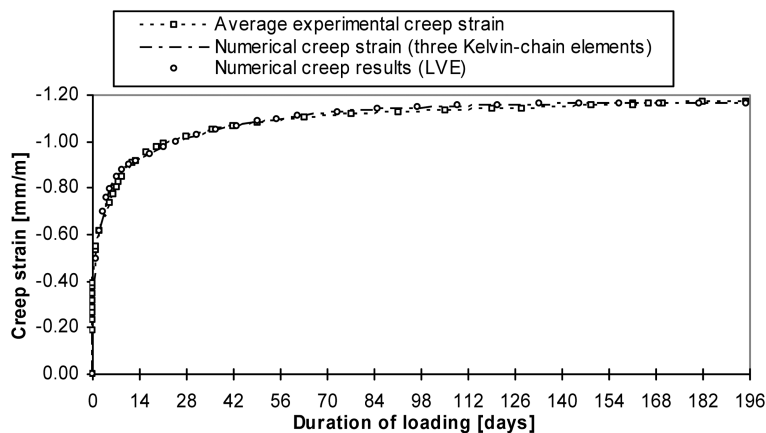


Fig. 11 Average experimental results and numerical results for creep strain for the first 196 days of loading

## 4. Conclusions

When a concrete structure is subjected to permanent loading it presents an immediate (elastic) deformation, which will be thereafter gradually increased by creep. The great majority of the phenomenological theories, numerical models and numerical methods of analysis, were developed for current concrete. Nowadays, recent progress in concrete mixing allows producing HSC, which exhibits different material properties and is able to be loaded sooner. Therefore, it becomes necessary to experimentally measure its time-dependent behaviour and also numerically verify the accuracy of existing models.

From the comparison between SH and LVE algorithms, it was concluded that SH was not suitable either for current or for high strength concrete. On the contrary, LVE is an unconditionally stable algorithm capable of simulating all proposed examples with accuracy. When provided with a sufficient number of Kelvin-chain elements, adequately adjusting the scalar creep function, LVE algorithm was able to simulate the practical case study.

## Acknowledgments

The authors are grateful to Pierre Pegon for his suggestions in several key moments during Cast3m implementation and to Vítor Dias da Silva for his support to the development of this work.

## References

- Acker, P. and Ulm, F.J. (2001), "Creep and shrinkage of concrete: physical origins and practical measurements", *Nucl. Eng. Des.*, **203**, 143-158.
- Argyris, J., St. Doltsinis, I. and Silva, V.D.D. (1992), "Constitutive modelling and computation of nonlinear viscoelastic solids. Part II: Application to orthotropic PVC-coated fabrics", *Comput. Method. Appl. M.*, **98**(2), 159-226.
- Bazant, Z.P. (1987), "Limitations of strain-hardening model for concrete creep", *Cement. Concrete Res.*, **17**(3), 505-509.
- Bazant, Z.P. and Prasannan, S. (1989), "Solidification theory for concrete creep 2. verification and application", *J. Eng. Mech.*, **115**(8), 1704-1725.
- Bazant, Z.P. and Wittmann, F.H. Eds. (1982), *Creep and shrinkage in concrete structures*, Numerical methods in Engineering, New York, John Wiley & Sons Ltd.
- Bockhold, J. (2007), "3D Material model for nonlinear basic creep of concrete", *Comput. Concrete*, **4**(2), 101-117.
- Borst, R.D. and Sluys, L.J. (1999), *Computational methods in non-linear solid mechanics*, Delft University of Technology, Delft.
- Coutinho, A.D.S. and Gonçalves, A. (1988), *Fabrico e propriedades do betão - Volume 3*, LNEC, Lisbon. (in Portuguese)
- Dias-da-Costa, D. (2006), *Comportamento Diferido do Betão. Modelação Numérica do Comportamento de Fluência de Vigas em Betão de Alta Resistência*, M.Sc. Thesis, Civil Engineering Department, University of Coimbra, Coimbra. (in Portuguese)
- England, G.L. (1967), "Numerical creep analysis applied to concrete structures", *ACI J. Proceedings*, **64**(6), 301-311.
- Fernandes, P.A.L. (2006), *Vigas de Grande Vão Pré-Fabricadas em Betão de Alta Resistência Pré-Esforçado - Viabilidade, Dimensionamento, Fabrico e Comportamento*, Ph.D. Thesis, University of Coimbra, Coimbra. (in Portuguese)

Portuguese)

- Freudenthal, A.M. and Roll, F. (1958), "Creep and creep recovery of concrete under high compressive stress", *ACI J. Proceedings*, **54-30**(66), 1111-1142.
- Gardner, N.J. and Tsuruta, H. (2004), "Is Superposition of creep strains valid for concretes subjected to drying creep?", *ACI Mater. J.*, **101**(5), 409-415.
- Gopalakrishnan, K.S. and Neville, A.M. and Ghali, A. (1969), "Creep poisson's ratio of concrete under multiaxial compression", *ACI J. Proceedings*, **66**(12), 1008-1020.
- Illston, J.M. (1968), "Components of creep in mature concrete", *ACI J. Proceedings*, **65**(3), 219-227.
- LNEC E 397 (1993), *Especificação E 397 - Betões. Determinação do módulo de elasticidade em compressão*, LNEC, Lisbon. (in Portuguese)
- LNEC E 398 (1993), *Especificação E 398 - Betões. Determinação da retracção e da expansão*, LNEC, Lisbon. (in Portuguese)
- LNEC E 399 (1993), *Especificação E 399 - Betões. Determinação da fluência em compressão*, LNEC, Lisbon. (in Portuguese)
- Neville, A. M. (1959), "Creep recovery of mortars made with different cements", *ACI J., Proceedings*, **56**, 167-174.
- Pichler, CH. (2008), "A multiscale creep model as basis for simulation of early-age concrete behavior", *Comput. Concrete*, **5**(2), 295-328.
- Ross, A.D. (1958), "Creep of concrete under variable stress", *ACI J. Proceedings*, **54**(3), 739-758.
- Yue, L.L. (1992), *Creep recovery of plain concrete under uniaxial compression*, Laboratorium Magnel voor Gewapend Beton, Ph. D. Thesis, University of Ghent, Ghent.
- Yue, L.L. and Taerwe, L. (1992), "Creep recovery of plain concrete and its mathematical-modeling", *Mag. Concrete Res.*, **44**(161), 281-290.
- Zienkiewicz, O.C. and Taylor, R.L. (1989), *The finite element method. Volume 1: basic formulation and linear problems*, Oxford, Butterworth-Heinemann.

CC